Journal of Contaminant Hydrology 138–139 (2012) 75–82

Contents lists available at SciVerse ScienceDirect

Journal of Contaminant Hydrology

journal homepage: www.elsevier.com/locate/jconhyd

A mathematical solution and analysis of contaminant transport in a radial two-zone confined aquifer

Yen-Ju Chen, Hund-Der Yeh *, Kai-Ju Chang

Institute of Environmental Engineering, National Chiao Tung University, 1001 University Road, Hsinchu 300, Taiwan

ARTICLE INFO

Article history:
Received 19 July 2011
Received in revised form 17 June 2012
Accepted 22 June 2012
Available online 29 June 2012

Keywords:
Radial dispersion
Contaminant transport
Skin effect
Laplace transform
Groundwater

ABSTRACT

An aquifer with a wellbore surrounded by a finite-thickness skin, such as a gravel pack, can be regarded as a radial two-zone system. In this study, a mathematical model is developed to describe contaminant transport in a radial two-zone confined aquifer system. The solution of the model equations can be used to delineate contaminant transport in such a two-zone aquifer system and to investigate the skin effect on the temporal and spatial concentration distribution. The present solution is shown to reduce to an existing solution for transport in a homogeneous aquifer in the case when there is no wellbore skin. The results predicted from the solution indicate that the skin effect has a significant impact on the concentration distribution at early time. But an abrupt change in the spatial concentration distribution may occur at the interface of the skin zone and aquifer formation zone. The results from a sensitivity analysis reveal that dispersivity in the formation zone has a more significant effect on the concentration distribution than do the effects of skin thickness and dispersivity in the skin zone.

1. Introduction

A skin zone that occurs around a well due to drilling practices or well completion may have properties that are different from the aquifer formation. This situation can be considered as a radial two-zone aquifer system with a finite-thickness skin adjacent to the aquifer region. Numerous studies have considered the influence of a skin zone on groundwater flow induced by various aquifer tests (e.g., Wen et al., 2011; Yang and Yeh, 2005, 2006), as well as on the estimation of hydrogeological properties (e.g., Chen and Yeh, 2009; Kabala, 2001; Yeh and Chen, 2007). It has been widely acknowledged that the existence of a skin zone affects the early-time head data near the well. However, little is known about the influence of a skin zone on contaminant transport in a radial two-zone aquifer system.

The radial contaminant transport problem represents the injection of a dissolved contaminant (e.g., waste water or treated water) into an aquifer, and several articles have examined this radial dispersion problem. Ogata (1958) first presented an analytical solution for the radial advection–dispersion equation (RADE) based on the Laplace transform and complex integral methods, though that study did not evaluate the integral solution. Hoopes and Harleman (1967) used a finite difference method to simulate solute transport in radial flow induced by a line source injection. Subsequently, both Dagan (1971) and Gelhar and Collins (1971) used perturbation methods to obtain approximate solutions for radial dispersion due to injection in a finite-radius well. For the radial dispersion problem, Tang and Babu (1979) developed an analytical solution expressed in terms of three integrals, including the combination of Bessel functions and/or modified Bessel functions, and an approximate solution in terms of the complementary error function. In addition, they also presented small-time and large-time solutions for the radial dispersion problem. Moench and Ogata (1981) solved the RADE by the Laplace transform technique. Their Laplace-domain solution was expressed in terms of Airy functions and inverted numerically to the time domain by the Stehfest (1970). Hsieh (1986) presented an analytical solution in terms of Airy

* Corresponding author. Tel.: +886 3 5731910; fax: +886 3 5725958.
E-mail address: hdyeh@mail.nctu.edu.tw (H.-D. Yeh).

0169-7722/$ – see front matter © 2012 Elsevier B.V. All rights reserved.
doi:10.1016/j.jconhyd.2012.06.006

functions for the radial dispersion problem, which was simpler than that of Tang and Babu (1979). These analytical solutions and approximate solutions serve as useful and efficient tools to predict solute concentration distributions in homogeneous aquifer systems. Recently, Zhan et al. (2009a, 2009b) dealt with solute transport in a layered system with two-dimensional transport in the aquifer and one-dimensional transport in the aquitard. The concentration distributions in the aquifer and aquitard were solved based on the Laplace transform technique along with the continuity requirements at the aquifer–aquitard interface. The Stehfest numerical inversion algorithm (1970) was used to obtain time-domain results. Though the presence of a wellbore skin is expected to affect the concentration distributions in the aquifer system, the dispersion problem in a radial two-zone aquifer, which accounts for the finite-thickness wellbore skin, has rarely been considered in the field of groundwater transport.

The purpose of this study is to develop a new mathematical solution for solute transport in a radial two-zone confined aquifer system. The case considered is of an injection well of finite radius that fully penetrates the aquifer. The Laplace-domain solution of the model is developed by the Laplace transform technique. Due to its complicated form, the time-domain solution is obtained by applying a numerical inversion. This solution is then used to investigate the effect of wellbore skin properties on the temporal and spatial concentration distribution in the aquifer system. In addition, the influence of dispersivities in the skin and formation zones as well as the skin thickness on predicted concentration values is assessed through a sensitivity analysis.

2. Methodology

2.1. Mathematical model and Laplace-domain solution

Fig. 1 shows the configuration considered; a well in a radial two-zone aquifer system. The injection well is located at the origin of the cylindrical coordinate system, which has a finite radius, r_w, and a screen that fully penetrates the aquifer. The contaminant is considered to be nonreactive and continuously released from the injection well with a constant concentration C_0. The confined aquifer has a finite thickness b and consists of two zones in the radial direction. The first zone, known as the wellbore-skin zone, is located around the injection well and has a thickness of r_1–r_w. The longitudinal dispersivity in the first zone is denoted by α_1. As indicated in Fig. 1, r_1 is the radial distance from the central line of the well to the outer radius of the wellbore skin. The second zone is known as the aquifer formation zone, which is homogeneous, isotropic, and of infinite lateral extent with a longitudinal dispersivity denoted by α_2. The contaminant concentrations in the first and second zones are denoted as C_1 and C_2, respectively.

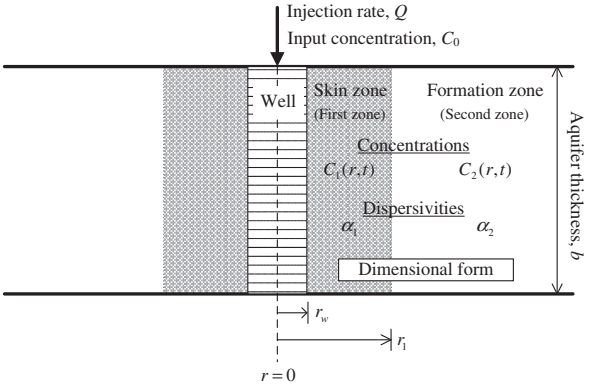

Fig. 1. Schematic diagram of an injection well in a radial two-zone aquifer system.

For convenience, the mathematical model is expressed in dimensionless form. The contaminant transport is dominated by radial advection and longitudinal dispersion in the two-zone system. The molecular diffusion coefficient is assumed to be negligible. The dimensionless concentration distribution in the skin zone is written as

$$\kappa\frac{\partial^2 G_1}{\partial\rho^2}-\frac{\partial G_1}{\partial\rho}=\rho\frac{\partial G_1}{\partial\tau},\quad \rho_w<\rho\le\rho_1,\quad \tau>0 \tag{1}$$

and in the aquifer formation zone as

$$\frac{\partial^2 G_2}{\partial\rho^2}-\frac{\partial G_2}{\partial\rho}=\rho\frac{\partial G_2}{\partial\tau},\quad \rho_1<\rho<\infty,\ \tau>0 \tag{2}$$

where $G_1=C_1/C_0$ and $G_2=C_2/C_0$ are the dimensionless concentrations in the skin and aquifer formation zones, respectively; $\kappa=\alpha_1/\alpha_2$ represents the ratio of longitudinal dispersivities in the skin and formation zones; $\rho=r/\alpha_2$ represents the dimensionless radial distance from the well; $\rho_w=r_w/\alpha_2$ and $\rho_1=r_1/\alpha_2$ are the dimensionless well radius and outer radius of the skin zone, respectively; $\tau=Qt/(2\pi bn\alpha_2^2)$ is the dimensionless time since injection of contaminant, and Q is the constant well injection rate, and n is the aquifer porosity. Both the skin and aquifer formation zones are initially free from contamination, expressed as

$$G_1(\rho,0)=G_2(\rho,0)=0,\quad \rho\ge\rho_w. \tag{3}$$

The boundary condition at the injection well is a constant concentration denoted as

$$G_1(\rho_w,\tau)=1,\quad \tau>0. \tag{4}$$

The aquifer formation is assumed to be free from contamination far from the well, where the concentration is written as

$$G_2(\infty,\tau)=0,\quad \tau>0 \tag{5}$$

The concentration and the flux at the interface between the skin and aquifer formation zones are continuous, expressed as

$$G_1(\rho_1,\tau)=G_2(\rho_1,\tau),\quad \tau>0 \tag{6}$$

and

$$\kappa\frac{\partial G_1(\rho_1,\tau)}{\partial\rho}=\frac{\partial G_2(\rho_1,\tau)}{\partial\rho},\quad \tau>0. \tag{7}$$

Taking the Laplace transform with respect to the dimensionless time τ of Eqs. (1) to (7) gives

$$\kappa\frac{d^2\bar{G}_1}{d\rho^2}-\frac{d\bar{G}_1}{d\rho}-\rho s\bar{G}_1=0,\quad \rho_w<\rho\le\rho_1 \tag{8}$$

$$\frac{d^2\bar{G}_2}{d\rho^2}-\frac{d\bar{G}_2}{d\rho}-\rho s\bar{G}_2=0,\quad \rho_1<\rho<\infty \tag{9}$$

$$\bar{G}_1(\rho_w,s)=\frac{1}{s} \tag{10}$$

$$\bar{G}_2(\infty,s)=0 \tag{11}$$

$$\bar{G}_1(\rho_1,s)=\bar{G}_2(\rho_1,s) \tag{12}$$

and

$$\kappa\frac{d\bar{G}_1(\rho_1,s)}{d\rho}=\frac{d\bar{G}_2(\rho_1,s)}{d\rho} \tag{13}$$

where $\bar{G}_1$ and $\bar{G}_2$ are the dimensionless Laplace-domain concentrations in the skin and formation zones, respectively, and s is the Laplace variable. The development of Eqs. (8) to (13) is given in Appendix A. The results for $\bar{G}_1$ and $\bar{G}_2$ are, respectively, given by

$$\bar{G}_1(\rho,s)=\frac{1}{s}\exp\left(\frac{\rho-\rho_w}{2\kappa}\right)\left\{\frac{Ai\left(Z_{1,\rho}\right)}{Ai\left(Z_{1,\rho_w}\right)}\left[1-Bi\left(Z_{1,\rho_w}\right)\frac{\nabla_1}{\nabla}\right]+Bi\left(Z_{1,\rho}\right)\frac{\nabla_1}{\nabla}\right\} \tag{14}$$

and

$$\bar{G}_2(\rho,s)=\frac{1}{s}\exp\left(\frac{\rho_1-\rho_w}{2\kappa}+\frac{\rho-\rho_1}{2}\right)\frac{Ai\left(Z_{2,\rho}\right)}{Ai\left(Z_{2,\rho_1}\right)}\times\left\{\frac{Ai\left(Z_{1,\rho_1}\right)}{Ai\left(Z_{1,\rho_w}\right)}\left[1-Bi\left(Z_{1,\rho_w}\right)\frac{\nabla_1}{\nabla}\right]+Bi\left(Z_{1,\rho_1}\right)\frac{\nabla_1}{\nabla}\right\} \tag{15}$$

where Ai(·) and Bi(·) are Airy functions. Other associated functions and variables are defined in Appendix A. The argument $Z_{1,\rho}$ is the abbreviation for the function $Z_1(\rho, s)$, as defined in Eq. (A.5). In addition, Z_{1,ρ_1} and Z_{1,ρ_w} are referred to as the function Z_1 by replacing ρ with their second indexes ρ_1 and ρ_w, respectively. Similarly, $Z_{2,\rho}$ and Z_{2,ρ_1} are the abbreviations for the functions $Z_2(\rho, s)$ and $Z_2(\rho_1, s)$, respectively, defined in Eq. (A.6).

2.2. Numerical evaluation

Numerical inversion and evaluation were carried out using a FORTRAN code with double precision accuracy. The Airy functions with argument x can be expressed in terms of the modified Bessel functions as (Abramovitz and Stegun, 1972)

$$Ai(x)=\frac{1}{\pi}\sqrt{\frac{x}{3}}K_{1/3}(\xi) \tag{16}$$

and

$$Bi(x)=\sqrt{\frac{x}{3}}\left[I_{-1/3}(\xi)+I_{1/3}(\xi)\right] \tag{17}$$

where $I(\cdot)$ and $K(\cdot)$ are the modified Bessel functions of the first and second kinds, respectively, with the argument $\xi=2/3\cdot x^{3/2}$. The derivatives of the Airy functions, which appear in Eqs. (A.13) and (A.14), are expressed by

$$Ai'(x)=-\frac{1}{\pi}\frac{x}{\sqrt{3}}K_{2/3}(\xi) \tag{18}$$

and

$$Bi'(x)=\frac{x}{\sqrt{3}}\left[I_{-2/3}(\xi)+I_{2/3}(\xi)\right]. \tag{19}$$

The functions $I(\cdot)$ and $K(\cdot)$ are calculated by the subroutines DCBIS and DCBKS of IMSL (2003a), respectively. The numerical inversion of Eqs. (14) and (15) to the time domain is achieved by the subroutine DINLAP of IMSL (2003b) which was developed based on the Crump algorithm (Chen et al., 1996).

2.3. Reduction to Moench and Ogata's solution

Moench and Ogata (1981) provided a Laplace-domain solution for the problem of radial dispersion with the contaminant injected into a well in an aquifer without the presence of wellbore skin. Their Laplace-domain solution is expressed as

$$\bar{G}(\rho,s)=\frac{1}{s}\exp\left(\frac{\rho-\rho_w}{2}\right)\frac{Ai\left(Y_\rho\right)}{Ai(Y_w)} \tag{20}$$

where

$$Y_\rho=\frac{4\rho s+1}{4s^{2/3}} \tag{21}$$

and

$$Y_w=\frac{4\rho_w s+1}{4s^{2/3}}. \tag{22}$$

Note that the present solution, i.e., Eqs. (14) and (15), can be reduced to Eq. (20) by setting $\rho_1=\rho_w$ and $\kappa=1$, i.e., $Z_1=Z_2=Y_\rho$, $Z_{1,\rho_1}=Z_{2,\rho_1}=Z_{1,\rho_w}=Y_w$, and $\nabla_1=0$.

2.4. Sensitivity analysis

Sensitivity analysis can be performed to examine the effect of changing the input parameters for model output, i.e., the concentration. The normalized sensitivity coefficients of U_{α_1}, U_{α_2} and U_{r_1} with respect to each of the parameters α_1, α_2 and r_1 indicate the relative importance of model parameters, which are expressed as (Liou and Yeh, 1997)

$$U_{\alpha_1}=\alpha_1\frac{\partial C}{\partial\alpha_1},\quad U_{\alpha_2}=\alpha_2\frac{\partial C}{\partial\alpha_2},\ \text{and}\ U_{r_1}=r_1\frac{\partial C}{\partial r_1}. \tag{23}$$

Note that these three coefficients have the same dimensions as concentration. Three new sensitivity coefficients are further introduced as

$$u_{\alpha_1}=\kappa\frac{\partial G}{\partial\kappa}=U_{\alpha_1}/C_0 \tag{24}$$

$$u_{\alpha_2}=\frac{1}{\rho_w}\cdot\frac{\partial G}{\partial\left(\frac{1}{\rho_w}\right)}=U_{\alpha_2}/C_0 \tag{25}$$

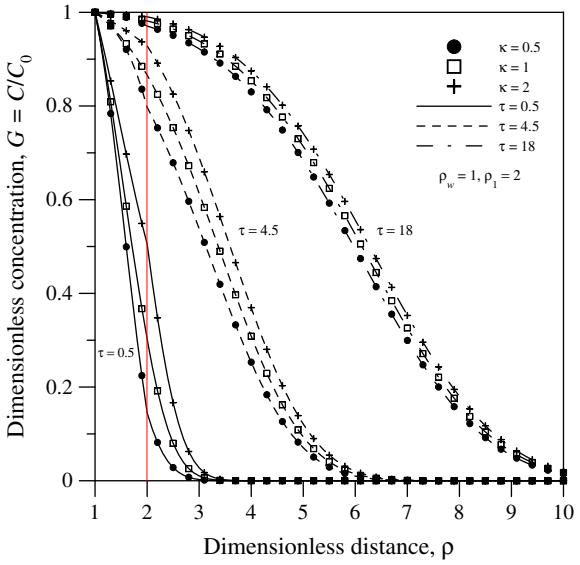

Fig. 2. Dimensionless concentration distributions for $\rho_w=1$, $\rho_1=2$, and $\kappa=0.5$, 1 and 2 when $\tau=0.5$, 4.5 and 18.

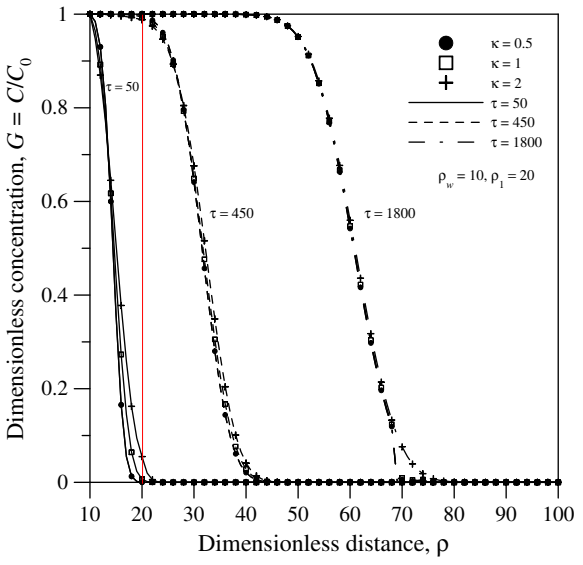

Fig. 3. Dimensionless concentration distributions for $\rho_w=10$, $\rho_1=20$, and $\kappa=0.5$, 1 and 2 when $\tau=50$, 450 and 1800.

and

$$u_{r_1}=\rho_1\frac{\partial G}{\partial \rho_1}=U_{r_1}/C_0 \tag{26}$$

where u_{α_1}, u_{α_2} and u_{r_1} represent the dimensionless normalized sensitivity coefficients of the dimensionless concentration with respect to the dimensionless parameters κ, $1/\rho_w$ and ρ_1, respectively. They are approximated by the finite-difference formulas as

$$u_{\alpha_1}\approx\kappa\frac{G(\kappa+\Delta\kappa)-G(\kappa)}{\Delta\kappa} \tag{27}$$

$$\begin{aligned}u_{\alpha_2}&\approx\alpha_2\frac{G[\rho_w(\alpha_2+\Delta\alpha_2),\rho_1(\alpha_2+\Delta\alpha_2),\kappa(\alpha_2+\Delta\alpha_2),\tau(\alpha_2+\Delta\alpha_2)]-G[\rho_w,\rho_1,\kappa,\tau]}{\Delta\alpha_2}\\&\approx\frac{1}{\rho_w}\frac{G[\rho_w(\alpha_2+\Delta\alpha_2),\rho_1(\alpha_2+\Delta\alpha_2),\kappa(\alpha_2+\Delta\alpha_2),\tau(\alpha_2+\Delta\alpha_2)]-G[\rho_w,\rho_1,\kappa,\tau]}{\Delta\left(\frac{1}{\rho_w}\right)}\end{aligned} \tag{28}$$

and

$$u_{r_1}\approx\rho_1\frac{G(\rho_1+\Delta\rho_1)-G(\rho_1)}{\Delta\rho_1} \tag{29}$$

where $\Delta\kappa$, $\Delta\alpha_2$ and $\Delta\rho_1$ denote small changes in the parameters, which are usually chosen as the parameter values multiplied by a factor of 10^{-3}. Thus, the following formulas are applied to calculate Eq. (28); i.e., $\rho_w(\alpha_2+\Delta\alpha_2)=\rho_w/1.001$, $\rho_1(\alpha_2+\Delta\alpha_2)=\rho_1/1.001$, $\kappa(\alpha_2+\Delta\alpha_2)=\kappa/1.001$, and $\tau(\alpha_2+\Delta\alpha_2)=\tau/1.001$.

3. Results and discussion

3.1. Effect of dispersivities in the formation zone

Fig. 2 displays the curves of dimensionless concentration versus dimensionless distance for $\rho_w=1$, $\rho_1=2$, and $\kappa=0.5$, 1 and 2 when $\tau=0.5$, 4.5 and 18. The case of $\kappa=1$ represents the absence of the skin zone. Furthermore, the cases of $\kappa=0.5$ and 2 represent the situations for $\alpha_1<\alpha_2$ and $\alpha_1>\alpha_2$, respectively. At the same distance, the highest dimensionless concentration is produced in the case of greatest κ at a specific time. Overall, the differences in dimensionless concentrations for $\kappa=0.5$, 1 and 2 decrease with time. The slopes of the dimensionless concentration curve are markedly different at the interface between the skin zone and formation zone ($\rho=2$) in the cases of $\kappa=0.5$ and 2 when $\tau=0.5$ and 4.5. The variations in the slope of the concentration curve may provide a diagnostic indication for the presence of the skin zone in the aquifer system, although it is recognized that such detailed data on concentration versus distance may rarely be available in the field.

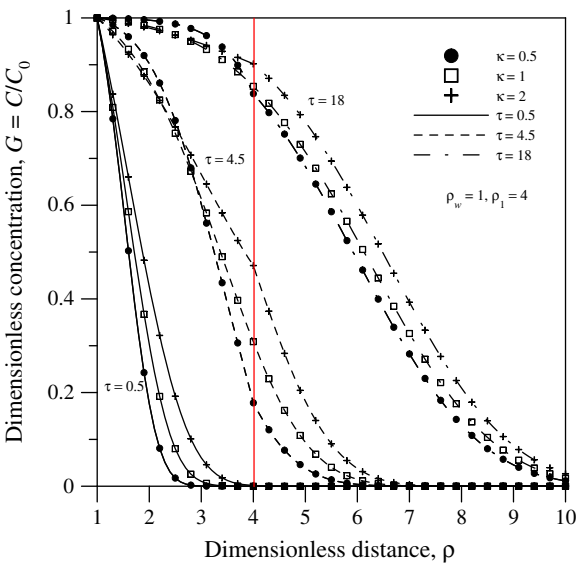

Fig. 4. Dimensionless concentration distributions for $\rho_w=1$, $\rho_1=4$, and $\kappa=0.5$, 1 and 2 when $\tau=0.5$, 4.5 and 18.

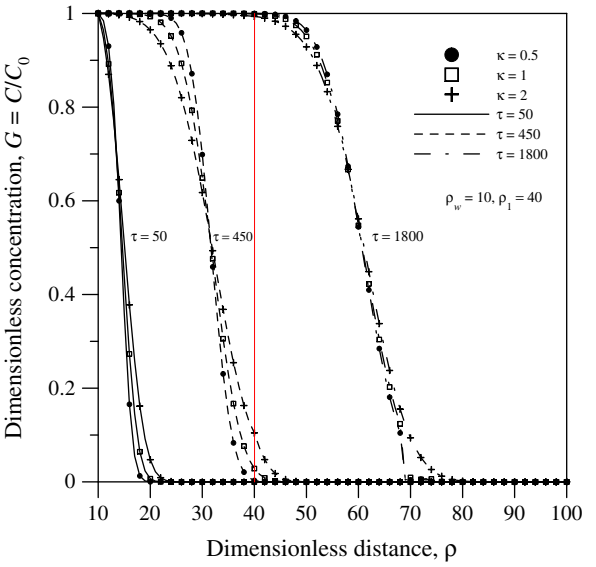

Fig. 5. Dimensionless concentration distributions for $\rho_w = 10$, $\rho_1 = 40$, and $\kappa = 0.5$, 1 and 2 when $\tau = 50$, 450 and 1800.

Fig. 3 shows the curves of dimensionless concentration versus dimensionless distance for $\rho_w = 10$, $\rho_1 = 20$, and $\kappa = 0.5$, 1 and 2 when $\tau = 0.5$, 450 and 1800, which is comparable with the corresponding curves in Fig. 2 to represent the case of smaller α_2 under the same well radius condition. Additionally, the dimensionless distance and time adopted in Fig. 3 are 10 and 100 times, respectively, those used in Fig. 2 for the same dimensional values. In Fig. 3, the differences in dimensionless concentrations for $\kappa = 0.5$, 1 and 2 are less significant than those in Fig. 2. The dimensionless concentration distributions for $\kappa = 0.5$, 1 and 2 closely coincide when the time is large ($\tau = 1800$). In contrast to Fig. 2, the highest dimensionless concentration does not always occur in the case of greatest κ at a specific time. Fig. 3 shows that these dimensionless concentration curves cross near $\rho = 14$ when $\tau = 50$, near $\rho = 30$ when $\tau = 450$, and near $\rho = 50$ when $\tau = 1800$. Fig. 3 also indicates that the plumes migrate shorter distances at corresponding times than those in Fig. 2.

3.2. Effect of skin thickness

Fig. 4 illustrates the dimensionless spatial concentration distributions for $\rho_w = 1$, $\rho_1 = 4$, and $\kappa = 0.5$, 1 and 2 when $\tau = 0.5$, 4.5 and 18 for the case of thicker skin. This figure indicates that the differences in dimensionless concentration for $\kappa = 0.5$, 1 and 2 are much more significant at larger distances from the well than those in Fig. 2. For the case of $\kappa = 0.5$, the dimensionless concentration does not change significantly at the early time ($\tau = 0.5$) as the skin thickness increases. In the case of $\kappa = 0.5$, the dimensionless concentration for $\rho_1 = 4$ (Fig. 4) is, however, much higher at short distances and lower at long distances for $\tau = 4.5$ and 18 than

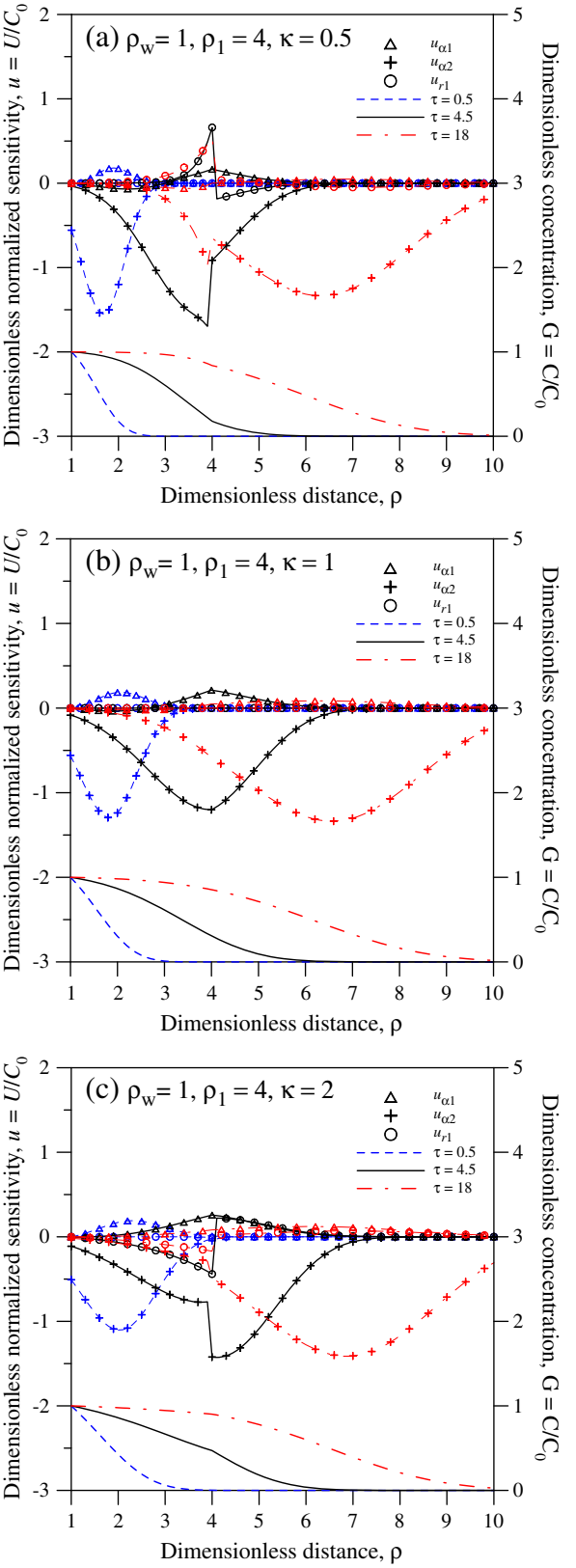

Fig. 6. Dimensionless concentration distributions and dimensionless normalized sensitivities (normalized sensitivities per C_0) of dimensionless concentration in response to the change in the parameters α_1, α_2 and r_1 for (a) $\kappa = 0.5$, (b) $\kappa = 1$, and (c) $\kappa = 2$ as well as $\rho_w = 1$ and $\rho_1 = 4$ when $\tau = 0.5$, 4.5 and 18.

the case of $\rho_1=2$ (Fig. 2). In contrast, the dimensionless concentration is lower at short distances but higher at long distances in the case of $\kappa=2$ (thicker-skin) than those in Fig. 2. Moreover, the spatial dimensionless concentration distributions for the case of $\kappa=2$ have distinct changes of slope at the interface between the skin and formation zones ($\rho=4$) when $\tau=4.5$ and 18.

Fig. 5 shows the dimensionless spatial concentration distributions for the case that the skin thickness is twice that in Fig. 3. The parameters used in Fig. 5 are $\rho_w=10$ and $\rho_1=40$ for $\kappa=0.5$, 1 and 2 when $\tau=50$, 450 and 1800. The increase in skin thickness did not distinctly affect the dimensionless concentration distribution at the early time ($\tau=50$). The differences in dimensionless concentration for $\kappa=0.5$, 1 and 2 are much more significant at $\tau=450$ and 1800 than those in Fig. 3. In comparison with Fig. 3, the same observation, as discussed in Fig. 4, applies to the case of $\kappa=0.5$, where the dimensionless concentration is much higher at short distances and lower at long distances for $\tau=450$ and 1800. In addition, a lower dimensionless concentration is predicted at short distances but a higher concentration is predicted at long distances in the case of $\kappa=2$ as the skin thickness increases. Figs. 4 and 5 show that the spatial concentration distributions change more sharply in the case of $\kappa=0.5$.

3.3. Sensitivity analysis

Fig. 6 illustrates the spatial dimensionless concentration distributions and the dimensionless normalized sensitivities of dimensionless concentration with respect to each of the parameters α_1, α_2 and r_1 for $\kappa=0.5$, 1 and 2 when $\rho_w=1$ and $\rho_1=4$. Generally, the values of dimensionless normalized sensitivity curves deviate from zero when the dimensionless concentration is between zero and one. The dimensionless concentration in response to the change in α_2 is more sensitive than those in α_1 and r_1. As shown in Fig. 6, positive perturbations in α_2 produce a negative concentration change. Fig. 6b indicates that the dimensionless concentration is insensitive to a change in r_1 when the skin is absent ($\kappa=1$). In other words, the change of skin thickness in such a case ($\kappa=1$) does not affect the dimensionless concentration since the dispersivities of the skin and formation zones are the same. In addition, the dimensionless concentration seems insensitive to the change in r_1 when the plume has not reached the formation zone, i.e., $\tau=0.5$, for $\kappa=0.5$ and 2, as displayed in Fig. 6a and c. These two figures also show that significant decreases or increases of the sensitivity curves occur at the interface of skin zone and formation zone, i.e., $\rho_1=4$. Fig. 6a shows that a positive perturbation in r_1 produces a positive concentration change within the skin zone and a negative change beyond the skin zone when $\tau=4.5$ and 18 for $\kappa=0.5$. In contrast, for the case of $\kappa=2$ shown in Fig. 6c, a positive perturbation in r_1 produces a negative change in the concentration within the skin zone and a positive change beyond the skin zone when $\tau=4.5$ and 18.

4. Conclusions

A mathematical model has been developed to describe the temporal and spatial dimensionless concentration distributions due to the continuous injection of a solute in a radial two-zone confined aquifer system. The Laplace-domain solution of the model equations was obtained in terms of Airy functions. A numerical Laplace inversion, called DINLAP of IMSL (2003b), was applied to evaluate the dimensionless concentration in the time domain. The present Laplace-domain solution for contaminant transport in a radial two-zone system can be reduced to Moench and Ogata (1981) if the wellbore skin is absent.

The present solution was applied to investigate the skin effect on the temporal and spatial concentration distributions. The differences in concentrations between the skin-affected cases and non-skin case become less significant at longer time but are much more notable when the dispersivity in the aquifer formation zone is large. In addition, there may be a sudden change in the slope of the concentration distribution at the interface between the skin zone and formation zone. An aquifer with a smaller dispersivity in the aquifer formation zone was shown to produce a shorter travel distance of the plume. Results from the sensitivity analysis indicated that the dimensionless concentration was more sensitive to the change of dispersivity in the formation zone than those of two other parameters, i.e., skin thickness and dispersivity in the skin zone.

Notation

The following symbols are used in this paper:

$Ai(\cdot)$	Airy function
b	aquifer thickness
b_1	coefficient in Eq. (A.7), which is defined in Eq. (A.9)
b_2	coefficient in Eq. (A.7), which is defined in Eq. (A.10)
$Bi(\cdot)$	Airy function
C_0	initial constant concentration injected into the well
C_1	contaminant concentration in the skin zone
C_2	contaminant concentration in the formation zone
d_1	coefficient in Eq. (A.8), which is defined in Eq. (A.11)
d_2	coefficient in Eq. (A.8), which is defined in Eq. (A.12)
G_1	dimensionless concentration in the skin zone, which is defined as $G_1=C_1/C_0$
G_2	dimensionless concentration in the formation zone, which is defined as $G_2=C_2/C_0$
$\bar{G}_1$	dimensionless Laplace-domain concentration in the skin zone
$\bar{G}_2$	dimensionless Laplace-domain concentration in the formation zone
$I(\cdot)$	modified Bessel function of the first kind
$K(\cdot)$	modified Bessel function of the second kind
n	aquifer porosity
Q	constant injection rate at the well
r_1	outer radius of the skin zone
r_w	radius of injection well
s	Laplace variable
u_{α_1}	normalized sensitivity coefficient of dimensionless concentration to κ, which is defined in Eq. (24)
u_{α_2}	normalized sensitivity coefficient of dimensionless concentration to $1/\rho_w$, which is defined in Eq. (25)
u_{r_1}	normalized sensitivity coefficient of dimensionless concentration to ρ_1, which is defined in Eq. (26)
U_{α_1}	normalized sensitivity coefficient of concentration to α_1, which is defined in Eq. (23)
U_{α_2}	normalized sensitivity coefficient of concentration to α_2, which is defined in Eq. (23)

U_{r_1} normalized sensitivity coefficient of concentration to r_1, which is defined in Eq. (23)
$\bar{U}_1$ function defined in Eq. (A.3)
$\bar{U}_2$ function defined in Eq. (A.4)
x argument
Y_ρ argument defined in Eq. (21)
Y_w argument defined in Eq. (22)
$Z_{1,\rho}$ abbreviation of the function $Z_1(\rho, s)$ defined in Eq. (A.5)
Z_{1,ρ_1} abbreviation of the function $Z_1(\rho_1, s)$, which can be calculated from Eq. (A.5)
Z_{1,ρ_w} abbreviation of the function $Z_1(\rho_w, s)$, which can be calculated from Eq. (A.5)
$Z_{2,\rho}$ abbreviation from the function $Z_2(\rho, s)$ defined in Eq. (A.6).
Z_{2,ρ_1} abbreviation of the function $Z_2(\rho_1, s)$, which can be calculated from Eq. (A.6)
α_1 longitudinal dispersivity in the skin zone
α_2 longitudinal dispersivity in the formation zone
∇ equation defined in Eq. (A.14)
∇_1 equation defined in Eq. (A.13)
κ ratio of longitudinal dispersivities in the skin and formation zones, which is defined as $\kappa = \alpha_1/\alpha_2$
ρ dimensionless radial distance from the well, which is defined as $\rho = r/\alpha_2$
ρ_w dimensionless well radius, which is defined as $\rho_w = r_w/\alpha_2$
ρ_1 dimensionless outer radius of the skin zone, which is defined as $\rho_1 = r_1/\alpha_2$
τ dimensionless time since contaminant injection, which is defined as $\tau = Qt/(2\pi bn\alpha_2^2)$
ξ argument defined as $\xi = 2/3 \cdot x^{3/2}$

Acknowledgments

This study was partly supported by the Taiwan National Science Council under the grants NSC 99-2221-E-009-062-MY3, NSC 100-2221-E-009-106, and NSC 101-3113-E-007-008. The authors would like to thank the editor, Dr. Greg B. Davis, for editing the manuscript and two anonymous reviewers for their valuable and constructive comments that help improve the clarity of our presentation.

Appendix A. Development of Eqs. (14) and (15)

Eqs. (8) and (9) can be rearranged as the Airy differential equations:

$$\frac{d^2\bar{U}_1}{dZ_1^{\,2}} - Z_1\bar{U}_1 = 0, \quad \rho_w < \rho \le \rho_1 \tag{A.1}$$

and

$$\frac{d^2\bar{U}_2}{dZ_2^{\,2}} - Z_2\bar{U}_2 = 0, \quad \rho_1 < \rho < \infty \tag{A.2}$$

where the new functions $\bar{U}_1$ and $\bar{U}_2$ are respectively related to $\bar{G}_1$ and $\bar{G}_2$ by

$$\bar{U}_1(\rho, s) = \exp\left(-\frac{\rho}{2\kappa}\right)\bar{G}_1(\rho, s) \tag{A.3}$$

and

$$\bar{U}_2(\rho, s) = \exp\left(-\frac{\rho}{2}\right)\bar{G}_2(\rho, s). \tag{A.4}$$

In addition, Z_1 and Z_2 are defined as

$$Z_1(\rho, s) = \left(\frac{s}{\kappa}\right)^{1/3}\left(\rho + \frac{1}{4\kappa s}\right) \tag{A.5}$$

and

$$Z_2(\rho, s) = \frac{4\rho s + 1}{4s^{2/3}}. \tag{A.6}$$

The general solutions to Eqs. (A.1) and (A.2) can be respectively expressed as

$$\bar{U}_1(\rho, s) = b_1 Ai(Z_1) + b_2 Bi(Z_1) \tag{A.7}$$

and

$$\bar{U}_2(\rho, s) = d_1 Ai(Z_2) + d_2 Bi(Z_2) \tag{A.8}$$

where the coefficients b_1, b_2, d_1 and d_2 are the constants determined by the associated boundary conditions (10) to (13). The coefficients are then obtained as

$$b_1 = \frac{1}{s}\exp\left(-\frac{\rho_w}{2\kappa}\right)\left[\frac{1}{Ai\left(Z_{1,\rho_w}\right)} - \frac{\nabla_1}{\nabla}\frac{Bi\left(Z_{1,\rho_w}\right)}{Ai\left(Z_{1,\rho_w}\right)}\right] \tag{A.9}$$

$$b_2 = \frac{1}{s}\exp\left(-\frac{\rho_w}{2\kappa}\right)\frac{\nabla_1}{\nabla} \tag{A.10}$$

$$d_1 = \frac{1}{s}\exp\left(\frac{\rho_1 - \rho_w}{2\kappa} - \frac{\rho_1}{2}\right)\frac{1}{Ai\left(Z_{1,\rho_w}\right)Ai\left(Z_{2,\rho_1}\right)}\left\{Ai\left(Z_{1,\rho_1}\right)\right. \tag{A.11}$$
$$\left. + \left[Ai\left(Z_{1,\rho_w}\right)Bi\left(Z_{1,\rho_1}\right) - Ai\left(Z_{1,\rho_1}\right)Bi\left(Z_{1,\rho_w}\right)\right]\frac{\nabla_1}{\nabla}\right\}$$

and

$$d_2 = 0 \tag{A.12}$$

where

$$\nabla_1 = \kappa^{2/3}Ai'\left(Z_{1,\rho_1}\right)Ai\left(Z_{2,\rho_1}\right) - Ai\left(Z_{1,\rho_1}\right)Ai'\left(Z_{2,\rho_1}\right) \tag{A.13}$$

and

$$\nabla = \kappa^{2/3}Ai\left(Z_{2,\rho_1}\right)\left[Ai'\left(Z_{1,\rho_1}\right)Bi\left(Z_{1,\rho_w}\right) - Ai\left(Z_{1,\rho_w}\right)Bi'\left(Z_{1,\rho_1}\right)\right] - Ai'\left(Z_{2,\rho_1}\right)\left[Ai\left(Z_{1,\rho_1}\right)Bi\left(Z_{1,\rho_w}\right) - Ai\left(Z_{1,\rho_w}\right)Bi\left(Z_{1,\rho_1}\right)\right]. \tag{A.14}$$

The notations Z_{1,ρ_w}, Z_{1,ρ_1} and Z_{2,ρ_1} are the abbreviations for the functions $Z_1(\rho_w, s)$, $Z_1(\rho_1, s)$ and $Z_2(\rho_1, s)$, respectively, which can be calculated from Eqs. (A.5) and (A.6). The Laplace-domain solutions of dimensionless concentrations in skin and formation zones, Eqs. (14) and (15), are then obtained by substituting Eqs. (A.7) and (A.8) into Eqs. (A.3) and (A.4), respectively.

References

Abramovitz, M., Stegun, I.A., 1972. Handbook of Mathematical Functions with Formulas, Graphs, and Mathematical Tables. Dover Publications, New York.

Chen, Y.J., Yeh, H.D., 2009. Parameter estimation/sensitivity analysis for an aquifer test with skin effect. Ground Water 47 (2), 287–299.

Chen, J.S., Liu, C.W., Chen, C.S., Yeh, H.D., 1996. A Laplace transform solution for tracer tests in a radially convergent flow field with upstream dispersion. Journal of Hydrology 183 (3–4), 263–275.

Dagan, G., 1971. Perturbation solutions of the dispersion equation in porous mediums. Water Resources Research 7 (1), 132–142.

Gelhar, L.W., Collins, M.A., 1971. General analysis of longitudinal dispersion in nonuniform flow. Water Resources Research 7 (6), 1511–1521.

Hoopes, J.A., Harleman, D.R.F., 1967. Dispersion in radial flow from a recharge well. Journal of Geophysical Research 72 (14), 3595–3607.

Hsieh, P.A., 1986. A new formula for the analytical solution of the radial dispersion problem. Water Resources Research 22 (11), 1597–1605.

IMSL, 2003a. IMSL Fortran Library User's Guide Math/Library Special Function, Version 5.0. Visual Numerics, Houston, Texas.

IMSL, 2003b. IMSL Fortran Library User's Guide Math/Library Volume 2 of 2, Version 5.0. Visual Numerics, Houston, Texas.

Kabala, Z.J., 2001. Sensitivity analysis of a pumping test on a well with wellbore storage and skin. Advances in Water Resources 24 (5), 483–504.

Liou, T.S., Yeh, H.D., 1997. Conditional expectation for evaluation of risk groundwater flow and solute transport: one-dimensional analysis. Journal of Hydrology 199 (3–4), 378–402.

Moench, A.F., Ogata, A., 1981. A numerical inversion of the Laplace transform solution to radial dispersion in a porous medium. Water Resources Research 17 (1), 250–252.

Ogata, A., 1958. Dispersion in porous media, Ph.D. dissertation, Northwestern University, Evanston, Illinois.

Stehfest, H., 1970. Numerical inversion of Laplace transforms. Communications of the ACM 13 (1), 47–49.

Tang, D.H., Babu, D.K., 1979. Analytical solution of a velocity dependent dispersion problem. Water Resources Research 15 (6), 1471–1478.

Wen, Z., Zhan, H.B., Huang, G.H., Jin, M.G., 2011. Constant-head test in a leaky aquifer with a finite-thickness skin. Journal of Hydrology 399 (3–4), 326–334.

Yang, S.Y., Yeh, H.D., 2005. Laplace-domain solutions for radial two-zone flow equations under the conditions of constant-head and partially penetrating well. Journal of Hydraulic Engineering ASCE 131 (3), 209–216.

Yang, S.Y., Yeh, H.D., 2006. A novel analytical solution for constant-head test in a patchy aquifer. International Journal for Numerical and Analytical Methods in Geomechanics 30, 1213–1230.

Yeh, H.D., Chen, Y.J., 2007. Determination of skin and aquifer parameters for a slug test with wellbore-skin effect. Journal of Hydrology 342 (3–4), 283–294.

Zhan, H.B., Wen, Z., Gao, G., 2009a. An analytical solution of two-dimensional reactive solute transport in an aquifer–aquitard system. Water Resources Research 45, W10501, http://dx.doi.org/10.1029/2008WR007479.

Zhan, H.B., Wen, Z., Huang, G., Sun, D., 2009b. Analytical solution of two-dimensional solute transport in an aquifer–aquitard system. Journal of Contaminant Hydrology 107, 162–174.